Guide to the heart: Differentiation of human pluripotent stem cells towards multiple cardiac subtypes

Schwach, V.

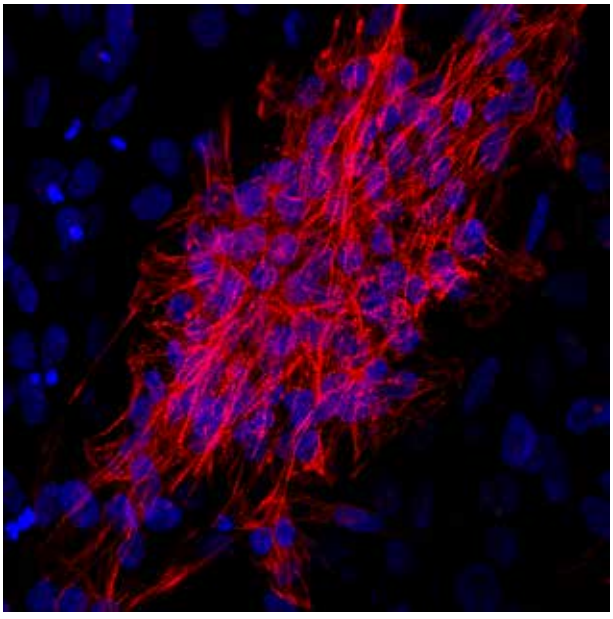

3

Chapter 3:

Atrial-like cardiomyocytes from human pluripotent stem cells are a robust preclinical model for assessing atrial-selective pharmacology

Harsha D. Devalla[1]; Verena Schwach[1]; John W. Ford[2]; James T. Milnes[2;] Said El-Haou[2]; Claire Jackson[2]; Konstantinos Gkatzis[1], David A. Elliott[3]; Susana M. Chuva de Sousa Lopes[1,4]; Christine L. Mummery[1]; Arie O. Verkerk[5] and Robert Passier[1]

[1]Department of Anatomy & Embryology, Leiden University Medical Center, Leiden, The Netherlands; [2]Xention Ltd, Cambridge, United Kingdom; [3]Murdoch Childrens Research Institute, Royal Children's Hospital, Melbourne, Australia; [4]Department for Reproductive Medicine, Ghent University Hospital, Ghent, Belgium; [5]Heart Failure Research Center, Academic Medical Center, University of Amsterdam, Amsterdam, The Netherlands.

EMBO Molecular Medicine, 7: 394–410 (2015)

Abstract

Drugs targeting atrial-specific ion channels, Kv1.5 or Kir3.1/3.4 are being developed as new therapeutic strategies for atrial fibrillation. However, current preclinical studies carried out in non-cardiac cell lines or animal models may not accurately represent the physiology of a human cardiomyocyte (CM). In the current study, we tested whether human embryonic stem cell (hESC)-derived atrial CMs could predict atrial-selectivity of pharmacological compounds. By modulating retinoic acid signaling during hESC differentiation, we generated atrial-like (hESC-atrial) and ventricular-like (hESC-ventricular) CMs. We found expression of atrial-specific ion channel genes, *KCNA5* (encoding K_v1.5) and *KCNJ3* (encoding Kir 3.1) in hESC-atrial CMs and further demonstrated that these ion channel genes are regulated by COUP-TF transcription factors. Moreover, in response to multiple ion channel blocker, vernakalant and K_v1.5 blocker, XEN-D0101, hESC-atrial but not hESC-ventricular CMs showed action potential (AP) prolongation due to a reduction in early repolarization. In hESC-atrial CMs, XEN-R0703, a novel Kir3.1/3.4 blocker restored the AP shortening caused by CCh. Neither CCh nor XEN-R0703 had an effect on hESC-ventricular CMs. In summary, we demonstrate that hESC-atrial CMs are a robust model for pre-clinical testing to assess atrial-selectivity of novel antiarrhythmic drugs.

Abbreviations:

CM – Cardiomyocyte; hESCs - Human embryonic stem cells; hESC-AM- Atrial-like cardiomyocyte; hESC-VM - Ventricular-like cardiomyocyte; RA - Retinoic acid

Introduction

Atrial fibrillation (AF) affects over 33 million people globally (Chugh et al., 2014) and is characterized by irregular atrial rhythm leading to a decline in atrial mechanical function. Untreated AF increases the risk of life-threatening complications such as stroke or heart failure (Marini et al., 2005; Wang et al., 2003). Current treatment options for rhythm control in AF include interventional therapy such as ablation or pharmacotherapy with antiarrhythmic drugs. The latter is the preferred treatment of early AF in individuals who prefer non-invasive treatment and as a follow-up therapy post-electrical cardioversion, to prevent recurrence of AF (Wann et al., 2011). However, existing antiarrhythmic agents lack atrial selectivity and pose the risk of inducing undesirable cardiac events, such as ventricular proarrhythmia (Dobrev and Nattel, 2010). In order to overcome this limitation, pharmaceutical industry has initiated design and development of compounds aimed at atrial-specific targets (Li et al., 2009; Milnes et al., 2012). The notorious difficulty in obtaining human cardiomyocytes (CMs) and propagating them in culture has precluded their use from many drug screening assays and instigated the use of alternative preclinical models. However, many of the current preclinical screening assays used in the identification of atrial-selective compounds are performed using either non-cardiac recombinant cell lines expressing a non-native ion channel or animal models. Both these models may not accurately represent the ion channel composition as well as physiology of a human CM and therefore have limitations in predicting drug responses on the human heart. Human pluripotent stem cell-derived CMs (hPSC-CMs) offer a human-based, physiologically-relevant model system for drug discovery and development strategies. Despite the suitability of these cells for cardiotoxicity testing and safety pharmacology (Braam et al., 2010; Navarrete et al., 2013), their application in validating novel drug candidates for AF requires cultures enriched in atrial-like CMs. Current protocols for cardiac differentiation of hPSCs, result in heterogeneous pools of CMs consisting predominantly of ventricular-like cells with a small percentage of atrial-like and nodal-like cells (Blazeski et al., 2012). Based on substantial evidence from *in vivo* and *in vitro* studies (Gassanov et al., 2008; Hochgreb et al., 2003; Niederreither et al., 2001; Zhang et al., 2011) indicating a role for retinoic acid (RA) in atrial specification, we hypothesized that RA would drive mesodermal progenitors from PSCs towards an atrial fate.

In the current study, we show that transcriptional and electrophysiological properties of human embryonic stem cell-derived atrial CMs (hESC-atrial CMs), generated by modulating RA signaling closely resemble that of native human atrial CMs. We also observed that transcription factors, COUP-TFI (NR2F1) and COUP-TFII (NR2F2) are robustly upregulated in response to RA during directed atrial differentiation. Short hairpin RNA (shRNA) mediated knockdown and chromatin immunoprecipitation (ChIP) of COUP-TFs identified that they regulate atrial-specific ion channel genes *KCNA5* (encoding $K_v1.5$) and *KCNJ3* (encoding Kir3.1). Furthermore, hESC atrial CMs express atrial-selective ion currents, I_{Kur} as well as $I_{K,ACh}$ and also respond to pharmacological compounds targeting ion channels that conduct these currents ($K_v1.5$ and Kir3.1/3.4 respectively).

Collectively, our data identifies a key role for COUP-TF transcription factors in RA-driven atrial differentiation and also demonstrates that hESC-atrial CMs are a robust model for predicting atrial-selectivity of novel pharmacological compounds during preclinical development.

Results

Treatment of differentiating hESCs with RA promotes atrial specification

A cocktail of cytokines (Fig. 1A) were used to initiate cardiac differentiation in NKX2.5$^{eGFP/+}$ hESCs as described previously (Elliott et al., 2011). To direct differentiating hESCs towards an atrial phenotype, timing and concentration of treatment with RA were carefully optimized (Fig. S1A-C). We hypothesized that specification of CM subtypes *in vitro* occurs post mesoderm formation and prior to the onset of cardiac progenitor stage. Accordingly, embryoid bodies (EBs) were supplemented with RA from day 4, just after the transient expression of early cardiac mesoderm marker, MESP1 until day 7, a time point at which key transcription factors such as NKX2.5, GATA4 and MEF2C, important for commitment and specification of cardiovascular lineages are activated (Fig. S1A). Adding low concentrations of RA (1-10 nmol/L) from day 4-7 enhanced cardiac differentiation as assessed by the percentage of GFP$^+$ cells at day 15 (Fig. S1B). On the other hand, treatment with high concentrations of RA (1 µmol/L) in the same time window resulted in GFP$^+$ EBs with reduced expression of the ventricular specific myosin gene, *MLC2V* (Fig. S1C). Therefore, treatment of differentiating hESCs with 1 µmol/L of RA from day 4-7 was considered to be most suitable for driving atrial differentiation. As a control, every experiment included parallel differentiating cultures treated with 0.002% DMSO (the final concentration in RA-treated cultures) from day 4-7 (Fig. 3.1A). Morphologically, RA-treated EBs were similar compared with control EBs (Fig. S1D) and contractile GFP$^+$ areas were observed in both groups at day 10 (Fig. 3.1B). Flow cytometry analysis of GFP expression at day 15 revealed a decrease in the proportion of NKX2.5 expressing cells upon treatment with RA. 65% of all cells expressed GFP in control differentiation while only 50% cells in RA-treated differentiation were GFP$^+$ (Fig. 1C; Fig. S1E). This data is consistent with earlier reports in zebrafish embryo which demonstrated that exposure of anterior lateral plate mesoderm to RA signaling restricts the size of the cardiac progenitor pool (Keegan et al, 2005). Also, EBs treated with RA during differentiation, displayed faster beating frequencies upon differentiation (Fig. S1F). Finally, immunofluorescence analysis of EBs from both control and RA-treated differentiations confirmed that the contractile GFP$^+$ areas expressed both NKX2.5 and the myofilament marker, ACTN2 (Fig. S1G). Adding low concentrations of RA (1-10 nmol/L) from day 4-7 enhanced

cardiac differentiation as assessed by the percentage of GFP^+ cells at day 15 (Fig. S1B). On the other hand, treatment with high concentrations of RA (1 µmol/L) in the same time window resulted in GFP^+ EBs with reduced expression of the ventricular specific myosin gene, *MLC2V* (Fig. S1C). Therefore, treatment of differentiating hESCs with 1 µmol/L of RA from day 4-7 was considered to be most suitable for driving atrial differentiation. As a control, every experiment included parallel differentiating cultures treated with 0.002% DMSO (the final concentration in RA-treated cultures) from day 4-7 (Fig. 3.1A). Morphologically, RA-treated EBs were similar compared with control EBs (Fig. S1D) and contractile GFP^+ areas were observed in both groups at day 10 (Fig. 3.1B). Flow cytometry analysis of GFP expression at day 15 revealed a decrease in the proportion of NKX2.5 expressing cells upon treatment with RA. 65% of all cells expressed GFP in control differentiation while only 50% cells in RA-treated differentiation were GFP^+ (Fig. 3.1C; Fig. S1E). This data is consistent with earlier reports in zebrafish embryo which demonstrated that exposure of anterior lateral plate mesoderm to RA signaling restricts the size of the cardiac progenitor pool (Keegan et al, 2005). Also, EBs treated with RA during differentiation, displayed faster beating frequencies upon differentiation (Fig. S1F). Finally, immunofluorescence analysis of EBs from both control and RA-treated differentiations confirmed that the contractile GFP^+ areas expressed both NKX2.5 and the myofilament marker, ACTN2 (Fig. S1G).

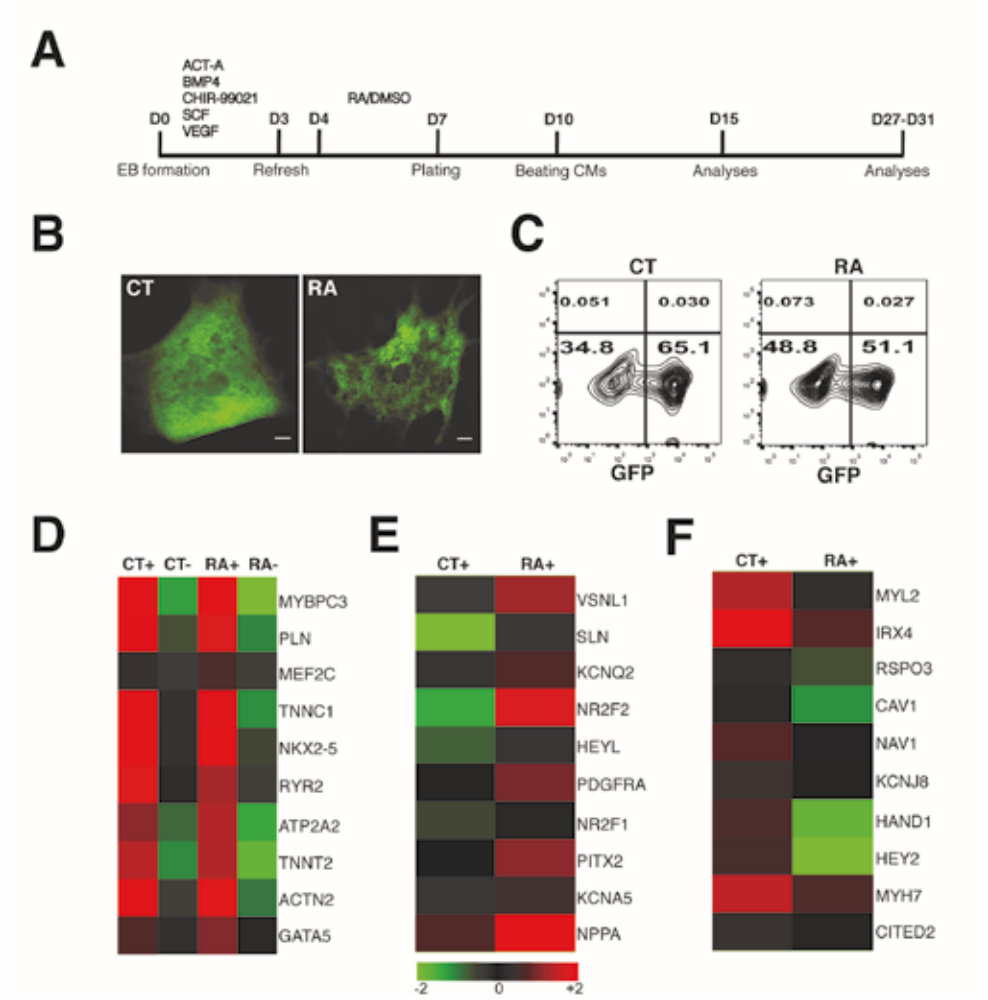

Figure 3.1: Treatment of differentiating hESCs with RA promotes atrial specification. A) Schematic of the cardiac differentiation protocol. Beating embryoid bodies (EBs) were observed at day 10. Differentiation efficiency in each experiment was assessed by flow cytometry (FC) for GFP at day 15. Further characterization of EBs derived from control (CT) and RA-treated (RA) cultures was carried out by transcriptional or functional analysis between days 27-31. B) GFP^+ EBs derived from CT and RA cultures at day 10; Scale bar: 100 µm. C) Representative FC plots depicting percentage of GFP^+ cells obtained at day 15, from CT and RA cultures in a typical experiment. D) Heat map demonstrating enrichment of cardiac genes in GFP^+ fractions (CT^+, RA^+) compared to GFP^- fractions (CT^-, RA^-) at day 31. E and F) Heat map of a select list of genes E) upregulated and F) downregulated in RA^+ compared to CT^+ at day 31. Fold change > 2.

Transcriptional profiling of CMs from RA-treated differentiations reveals an upregulation of atrial and downregulation of ventricular markers

To study gene expression in CMs resulting from control and RA-treated conditions, cells were sorted on the basis of NKX2.5^{eGFP}. GFP$^+$ and GFP$^-$ fractions from control (CT$^+$/CT$^-$) and RA-treated EBs (RA$^+$/RA$^-$) isolated at day 31 post-differentiation, were assessed by microarray and quantitative PCR (qPCR). Expression of contractility genes, *TNNC1* and *TNNT2*; calcium handling genes, *RYR2* and *ATP2A2*; cardiac transcription factors, *MEF2C* and *NKX2.5* were enriched in both CT$^+$ and RA$^+$ pools compared with CT$^-$ and RA$^-$ populations, indicating efficient purification of CMs (Fig. 3.1D). A heat map of GFP$^+$ and GFP$^-$ samples also demonstrates strong correlation within each group (Fig. S2A). Microarray analysis demonstrated upregulation of atrial markers such as *SLN, HEYL, PITX2* and *NPPA* (Fig. 3.1E) while ventricular markers such as *MYL2, IRX4, HAND1* and *HEY2* were downregulated in RA$^+$ CMs (Fig. 3.1F). Measuring expression levels of selected targets by quantitative qPCR further validated the microarray data in which expression of *NKX2.5* and *TNNT2* was significantly higher in GFP$^+$ fractions (Fig. 3.2A). qPCR also confirmed upregulation of atrial and downregulation of ventricular transcripts in RA$^+$ CMs (Fig. 3.2B-C). In order to compare the expression profile of CT$^+$ and RA$^+$ CMs at day 31 with that of human heart, we included atrial and ventricular tissue samples of a 15 week-old fetal heart for microarray analysis. A total of 151 genes showed increased expression of more than 2-fold in CT$^+$ group compared to RA$^+$. 32% of these genes (49 out of 151) were preferentially expressed in human ventricles, whereas only 8% (13 out of 151) could be identified in the group of genes that were enriched in the human atria (Fig. 2D). On the other hand, 292 genes showed increased expression of more than 2-fold in RA$^+$ group compared to CT$^+$. 31% of the genes (92 out of 292) with enriched expression in RA$^+$ group were preferentially expressed in the human atria while a mere 8% (23 out of 292) of these genes were expressed in the human ventricles (Fig. 3.2E). Gene lists in Venn diagrams (Fig. 3.2D-E) are included in Expanded view table S1. Pie charts illustrating the cellular localization and molecular function of genes enriched in CT$^+$ and RA$^+$ groups are shown in Fig. S2B-C. Gene ontology (GO) analysis of microarray data was performed with ConsensusPathDB-human and terms satisfying a cutoff of $p<0.01$ were considered enriched. GO terms related to four major classes- cardiovascular development, muscle development, developmental

process and adhesion were overrepresented in both groups (Fig. 3.2F). In the category of cardiovascular development, GO terms such as appendage development, cardiac atrium development and cardiac septum development were enriched in RA$^+$ CMs while cardiac ventricle development, ventricular septum formation and heart trabecular formation were enriched in CT$^+$ CMs (Expanded view table S2). Therefore, the transcriptional profile of RA$^+$ CMs suggested a fetal atrial-like gene expression pattern compared with control CMs, which expressed higher levels of ventricular transcripts.

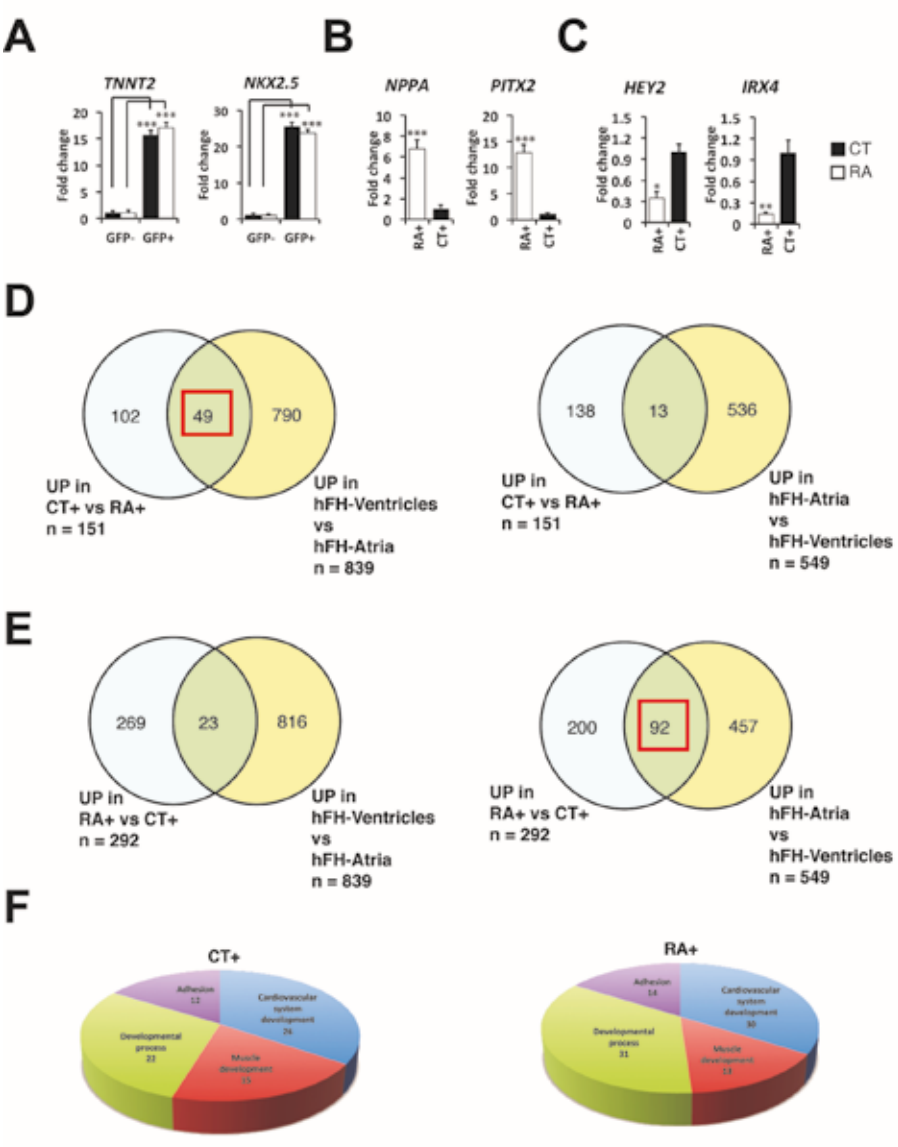

Figure 3.2: Transcriptional analysis of CT^+ and RA^+ CMs. qPCR of selected transcripts at day 31 to validate A) enrichment of cardiac markers in GFP^+ fractions against GFP^- fractions, B) upregulation of atrial and C) downregulation of ventricular genes in RA^+ compared to CT^+; (n=3) Venn diagram to illustrate overlap of gene lists upregulated (UP) in D) CT^+ CMs and E) RA^+ CMs with genes expressed in atria and ventricles of 15 week-old fetal heart. Red square indicates higher overlap of CT^+ with gene list of fetal ventricles or higher overlap of RA^+ with gene list of fetal atria F) Pie chart illustrates major classes of gene ontology terms enriched in gene lists upregulated in CT^+ and RA^+ CMs. *P<0.05, **P<0.01, ***P<0.001 by unpaired t-test.

AP characterization of CMs generated from RA-treated differentiations establishes their atrial-like phenotype

To study the electrical phenotype of CMs treated with RA during differentiation, we measured APs of dissociated single cells using the patch-clamp method (Fig. 3.3). Representative APs stimulated at 1 Hz are shown in Fig. 3.3B. The AP of a CM treated with RA during differentiation (RA) depicts an AP with a fast phase-1 repolarization and a plateau phase with a more negative potential compared to a control (CT) CM (Fig. 3.3B). Average RMP (Fig. 3.3C) and dV/dt_{max} (Fig. 3.3D) did not differ significantly between the two groups. In particular, APs of RA CMs had a significantly lower APA_{max} (Fig. 3.3C). They also repolarized faster resulting in significantly lower APAplat (Fig. 3.3C) and shorter APD_{20}, APD_{50} and APD_{90} (Fig. 3.3E). A scatter-plot of individual APA_{plat} values clearly shows that the plateau amplitudes of individual cells in the RA group were typically <80 mV whereas those in the CT group were >80 mV (Fig. 3.3F). The AP differences between the two groups were also consistent when the cells were paced at higher frequencies (Fig. 3.3G and 3.3H). Of 25 cells measured from the control group, about 80% (of 25 cells) displayed ventricular-like action potential properties while about 85% (of 26 cells) in the RA treatment group showed atrial-like action potential properties. We observed a very small percentage (<1 %) of nodal-like cells in both the groups. The differences observed in AP duration and APA_{plat} between RA and CT CMs closely matched the AP differences observed between atrial and ventricular CMs *in vivo* (Nerbonne and Kass, 2005). Taken together, gene expression signature and electrophysiological properties demonstrated that CMs treated with RA during differentiation displayed atrial-like phenotype (hereby referred to as hESC-atrial CMs) while control CMs resembled ventricular-like cells (hereby referred to as hESC-ventricular CMs).

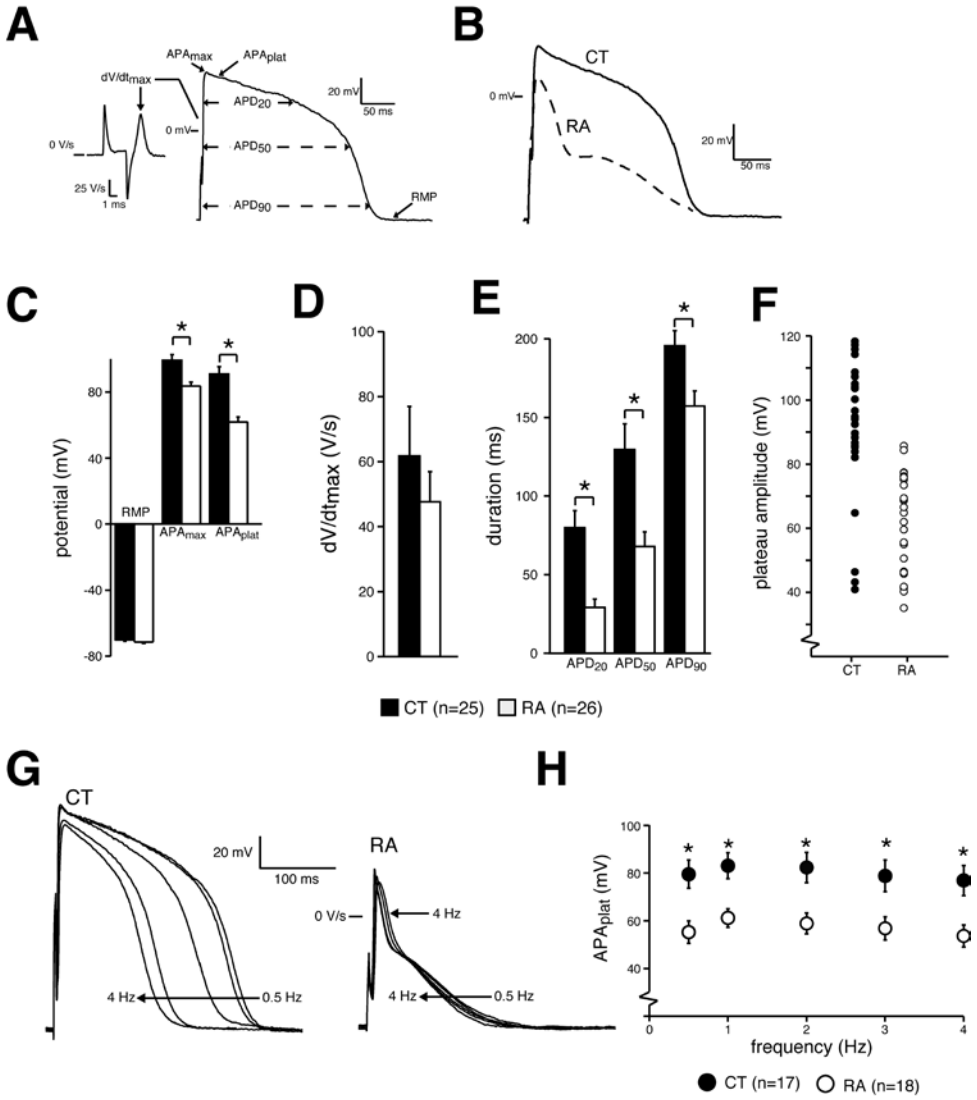

Figure 3.3: AP characterization of CMs generated from control and RA-treated differentiations. A) AP illustrating the analysed parameters B) Representative APs of day 31 CMs from Control (CT) and RA-treated (RA) groups at 1 Hz. C) RMP, APA_{max} and APA_{plat} D) dV/dt_{max} E) APD_{20}, APD_{50} and APD_{90} of CT and RA CMs. F) Plot showing all measured APA_{plat} values of CT and RA CMs. G) Representative APs of CT and RA CMs at 0.5-4 Hz. H) Average APA_{plat} at 0.5-4 Hz. Please note that the AP differences in morphology are present at all measured frequencies. AP = action potential; APA_{max} = maximum AP amplitude, APA_{plat} = AP plateau amplitude; APD_{20}, APD_{50}, and APD_{90} = AP duration at 20, 50, and 90% repolarization, respectively; CMs = cardiomyocytes;

dV/dt_{max} = maximum upstroke velocity; RMP = resting membrane potential. * P <0.05 by Unpaired t-test or Mann-Whitney rank sum test for Fig. 3.3C-E; Two-Way Repeated Measures ANOVA followed by pairwise comparison using the Student-Newman-Keuls test for Fig. 3.3H.

COUP-TFI and COUP-TFII are upregulated in response to retinoic acid and their expression persists in differentiated hESC-atrial CMs

Transcriptional profiling experiments revealed that orphan nuclear receptor transcription factors, COUP-TFI (NR2F1) and COUP-TFII (NR2F2) are highly upregulated in hESC-atrial CMs. Based on previous reports by others indicating the involvement of COUP-TFs in RA signaling (Jonk et al., 1994; Wees et al., 1996), we postulated that these genes might play a central role downstream of RA during atrial differentiation. This hypothesis was further supported by atrial-specific expression of Coup-tfII in the mouse and severe atrial abnormalities observed in the loss-of-function mouse mutant (Pereira et al., 1999). A more recent study found that Coup-tfII regulates atrial identity in the mouse heart (Wu et al., 2013). In order to determine the dynamics of COUP-TF expression following RA treatment, expression levels of both COUP-TFI and II were analyzed by qPCR at different time points and compared to control EBs. COUP-TFs were induced within 24 hours of treatment with RA followed by dramatic increase in expression thereafter. A line graph plotting the relative mRNA levels of COUP-TFI and II between control and RA-treated groups shows striking differences indicating that addition of RA induced the expression of these orphan nuclear receptor transcription factors (Fig. 3.4A-B). The expression of COUP-TFs was maintained in differentiated CMs at day 31. COUP-TFI was expressed 20-fold higher and COUP-TFII was enriched over 30-fold in hESC-atrial CMs compared to hESC-ventricular CMs (Fig. 3.4A-B). Antibodies selectively binding to COUP-TFI or COUP-TFII were used to verify the expression of these proteins. While GFP^+ areas in hESC-ventricular CMs at day 25 showed relatively low expression of COUP-TFI and COUP-TFII, hESC-atrial CMs showed robust expression of these transcription factors (Fig. 3.4C-D).

To confirm our *in vitro* findings, which identified high levels of COUP-TFs in hESC-atrial CMs, we sought to verify the expression of COUP-TFI and COUP-TFII in the human heart. Previous studies by others have reported preferential expression of Coup-tfII in the atrial myocardium of the mouse heart (Pereira et al., 1999) but no data is available for Coup-tfI. QPCR

identified significantly higher mRNA levels of COUP-TFI and COUP-TFII in the atria as opposed to ventricles in both human fetal and adult heart (Fig. S3A-B). In accordance with the mRNA expression levels, COUP-TFI protein showed nuclear localization in the myocardium of the atrial chambers stained with TNNI3 (Fig. S3D-E) while no expression was detected in the myocardium of ventricles (Fig. S3F-G) or elsewhere in two of the analyzed hFHs at 12 weeks of gestation. Similarly, strong expression of COUP-TFII was observed in the TNNI3-positive myocardium of the atria (Fig. S3H-I) while no expression was found in the ventricular myocardium (Fig. S3J-K) of the hFH. Collectively, expression and histochemical analysis in human fetal hearts demonstrate that COUP-TFI and II are indeed expressed in the atrial myocardium of the human heart as observed in hESC-atrial CMs *in vitro*.

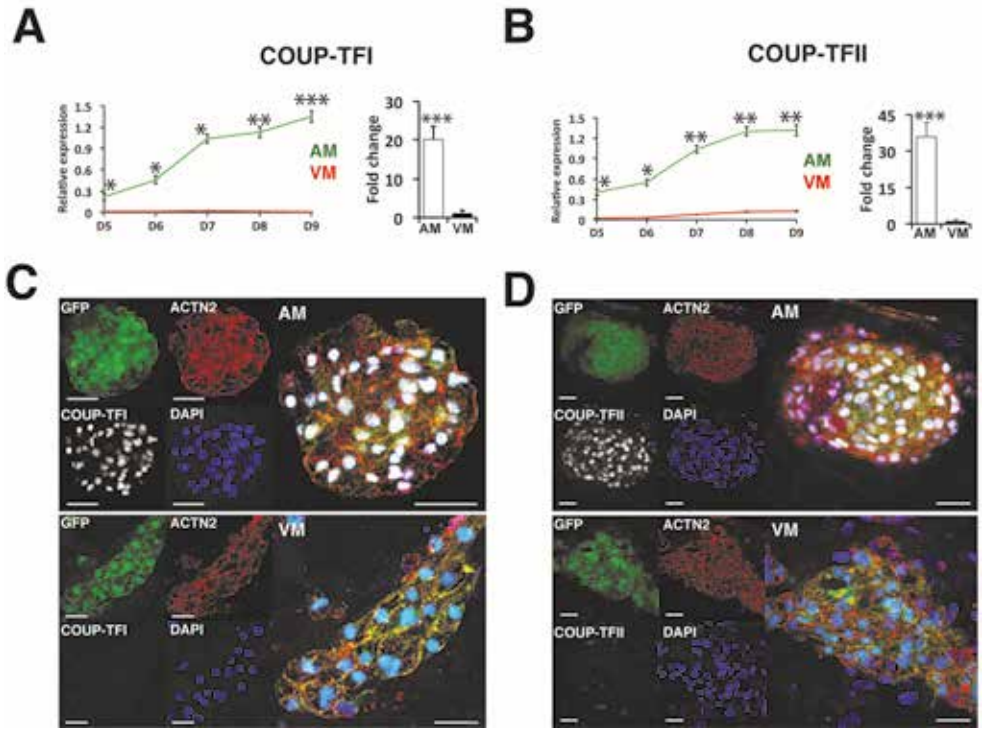

Figure 3.4: Retinoic acid induces COUP-TFI and COUP-TFII during atrial differentiation. A and B) Line plot illustrating relative mRNA levels of A) COUP-TFI B) COUP-TFII in VM and AM differentiations from day 5 through day 9 (left) and in GFP+ CMs at day 31 (right); n=3. C) COUP-TFI immunofluorescence at day 31 in AM (top) and VM (bottom) D) COUP-TFII immunofluorescence at day 31 in AM (top) and VM (bottom). Scale bars: 40 μm; CT = control differentiation; hESC-atrial (AM); hESC-ventricular (VM). *P<0.05, **P<0.01, ***P<0.001 by unpaired t-test.

COUP-TFs regulate expression of atrial-specific potassium channel genes, *KCNA5* and *KCNJ3*

To investigate whether COUP-TFs have an essential role in differentiated CMs, we used shRNAs to knockdown COUP-TFI or COUP-TFII in hESC-atrial CMs and studied whether they regulate atrial-specific ion channel genes. Lentiviral pLKO.1 constructs containing five different shRNA sequences each (Expanded view table S4), for COUP-TFI and COUP-TFII (Fig. S4A-C) were tested in hESC-atrial CMs. Two COUP-TFI-shRNAs (#2; #4) and two COUP-TFII-shRNAs (#7; #10) gave efficient knockdown as assessed by qPCR (Fig. S4D) and were selected for further experiments. Transduction of COUP-TFI-shRNA or COUP-TFII shRNA in hESC-atrial CMs resulted in 70-75% reduction of the corresponding mRNA in comparison with cells transduced with the scrambled-shRNA (Fig. 3.5A-B). Knockdown of COUP-TFI and COUP-TFII protein following shRNA transduction was confirmed by western blot (Fig. S4E). hESC-atrial CMs transduced with scrambled-shRNA or COUP-TF-shRNAs maintained their cardiac phenotype. Knockdown of COUP-TFI or COUP-TFII in hESC-atrial CMs did not affect GFP or *cTNT* expression (Fig. S5A-B). Furthermore, shRNA targeted knockdown of *COUP-TFI* did not affect the expression of *COUP-TFII* and vice versa (Fig. 3.5A-B). However, knockdown of COUP-TFI or COUP-TFII in hESC-atrial CMs led to significant decrease in the expression of *KCNA5* (Fig. 3.5C-D). Similarly, knockdown of COUP-TFII decreased the expression of ion channel genes *KCNJ3* and *KCNJ5* (Fig. 3.5D). Although, there was a small reduction in the expression of *KCNJ3* and *KCNJ5* in hESC-atrial CMs with decreased COUP-TFI expression (Fig. 3.5C), it did not reach significance. To test whether the atrial-enriched ion channel genes *KCNA5* and *KCNJ3* are direct targets of COUP-TFs, we performed ChIP-qPCR assays using day 30 hESC-atrial CMs. COUP-TF genes regulate transcription by interacting with direct repeats (DRs) of hormone responsive elements with various spacings but show highest affinity to DR sequences separated by 1 nucleotide (DR1). Bioinformatic analysis of promoter regions of human *KCNA5* and *KCNJ3* by Genomatix-MatInspector revealed potential binding sites of the Genomatix-defined NR2F matrix family (Fig. S5). The promoter region of *KCNA5* harbored two plausible NR2F binding sites (Fig. 3.5E) and analysis of immunoprecipitated DNA with primers designed around site 1 confirmed binding of both COUP-TFI and II (Fig. 3.5G). Promoter analysis of *KCNJ3* identified several putative NR2F binding sites (Fig. 3.5F) and qPCR for region encompassing site 1 confirmed interaction of both COUP-TFs (Fig. 3.5H).

Taken together, this data suggests that COUP-TFI and COUP-TFII play a pivotal role in regulating ion channel genes responsible for unique electrophysiological phenotype of human atrial cells.

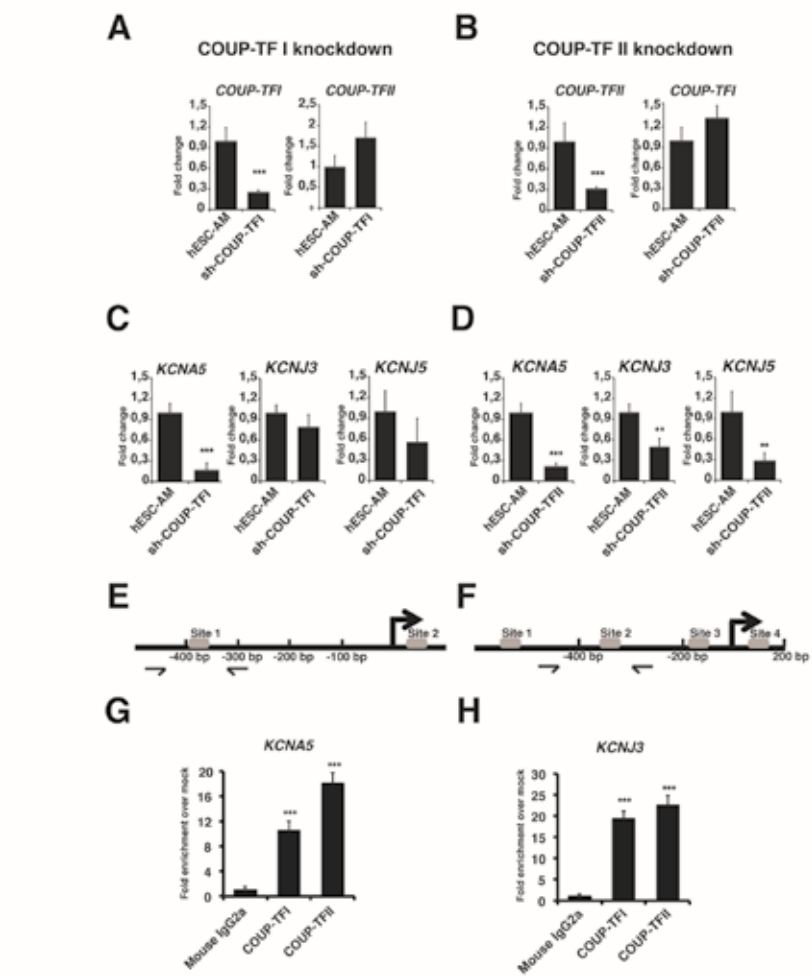

Figure 3.5: COUP-TFs regulate atrial-specific ion channel genes, *KCNA5* and *KCNJ3*. A and B) mRNA expression of COUP-TFI and COUP-TFII following shRNA-mediated knockdown of A) COUP-TFI or B) COUP-TFII in hESC-atrial cardiomyocytes (AM) at day 30. C-D) mRNA expression of ion channel genes *KCNA5*, *KCNJ3* and *KCNJ5* after knockdown of C) COUP-TFI or D) COUP-TFII in AM at day 30. E and F) Schematic of NR2F binding sites in E) *KCNA5* and F) *KCNJ3* promoters. G and H) ChIP-qPCR analysis at day 30 shows enriched binding of COUP-TFI and COUP-TFII to the promoter region of G) *KCNA5* and H) *KCNJ3*, compared to IgG in AM. *P<0.05, **P<0.01, ***P<0.001 by unpaired t-test.

Atrial-specific currents I_{Kur} and $I_{K,ACh}$ are functional in hESC-atrial CMs

The potassium ion channels $K_v1.5$ and the Kir3.1/3.4 are more abundant in human atrial than in ventricular CMs (Krapivinsky et al., 1995; Wang et al., 1993) and are responsible for functional differences between the two chambers. $K_v1.5$, encoded by the gene *KCNA5*, conducts the ultrarapid delayed rectifier K^+ current, I_{Kur}, which is a major repolarizing current in the human atrium. Heteromultimers of K^+ channels Kir3.1/3.4 encoded by the genes *KCNJ3* and *KCNJ5* respectively, conduct the acetylcholine-activated current $I_{K,ACh}$ in the human atria. We observed significantly higher mRNA expression of both *KCNA5* and *KCNJ3* in hESC-atrial CMs compared with hESC-ventricular CMs, in a manner similar to human atrial tissue (in comparison with human adult ventricular tissue) (Fig. 3.6A). We next assessed the current densities of I_{Kur} and $I_{K,ACh}$ in hESC-ventricular and hESC-atrial CMs. I_{Kur}, measured as the current sensitive to 50 µmol/L 4-AP (Wang et al., 1993) was clearly present in hESC-atrial CMs but absent in hESC-ventricular CMs (Fig. 3.6B). $I_{K,ACh}$, measured as the current evoked by the muscarinic agonist, CCh (10 µmol/L) was also present in hESC-atrial CMs but could not be detected in hESC-ventricular CMs (Fig. 3.6C). Thus, hESC-atrial CMs have substantially higher I_{Kur} and $I_{K,ACh}$ densities, consistent with the greater mRNA expression of *KCNA5* and *KCNJ3*. Lastly, we evaluated the contribution of I_{Kur} and $I_{K,ACh}$ in the APs of hESC-atrial and hESC-ventricular CMs. Blocking I_{Kur} by 4-AP (50 µmol/L) reduced phase-1 repolarization resulting in AP prolongation and an increase in APA_{plat} in hESC-atrial but not hESC-ventricular CMs (Fig. 3.6D; Expanded view table S5). These effects of I_{Kur} block observed in hESC-atrial CMs, confirmed its functional presence and are consistent with the effects reported in freshly isolated human atrial CMs (Wang et al., 1993). On the other hand, activation of $I_{K,ACh}$ by CCh resulted in hyperpolarization of the RMP in hESC-atrial CMs but not in hESC-ventricular CMs (Fig. 3.6E; Expanded view table S5). The effects of $I_{K,ACh}$ activation on the AP of hESC-atrial CMs are consistent with findings in isolated human atrial myocytes (Koumi et al., 1994. These results suggest that hESC-atrial CMs derived from RA-treated differentiations possess functional I_{Kur} and $I_{K,ACh}$ currents and might therefore be a suitable model for testing drug responses of pharmacological compounds selective for atrial cells.

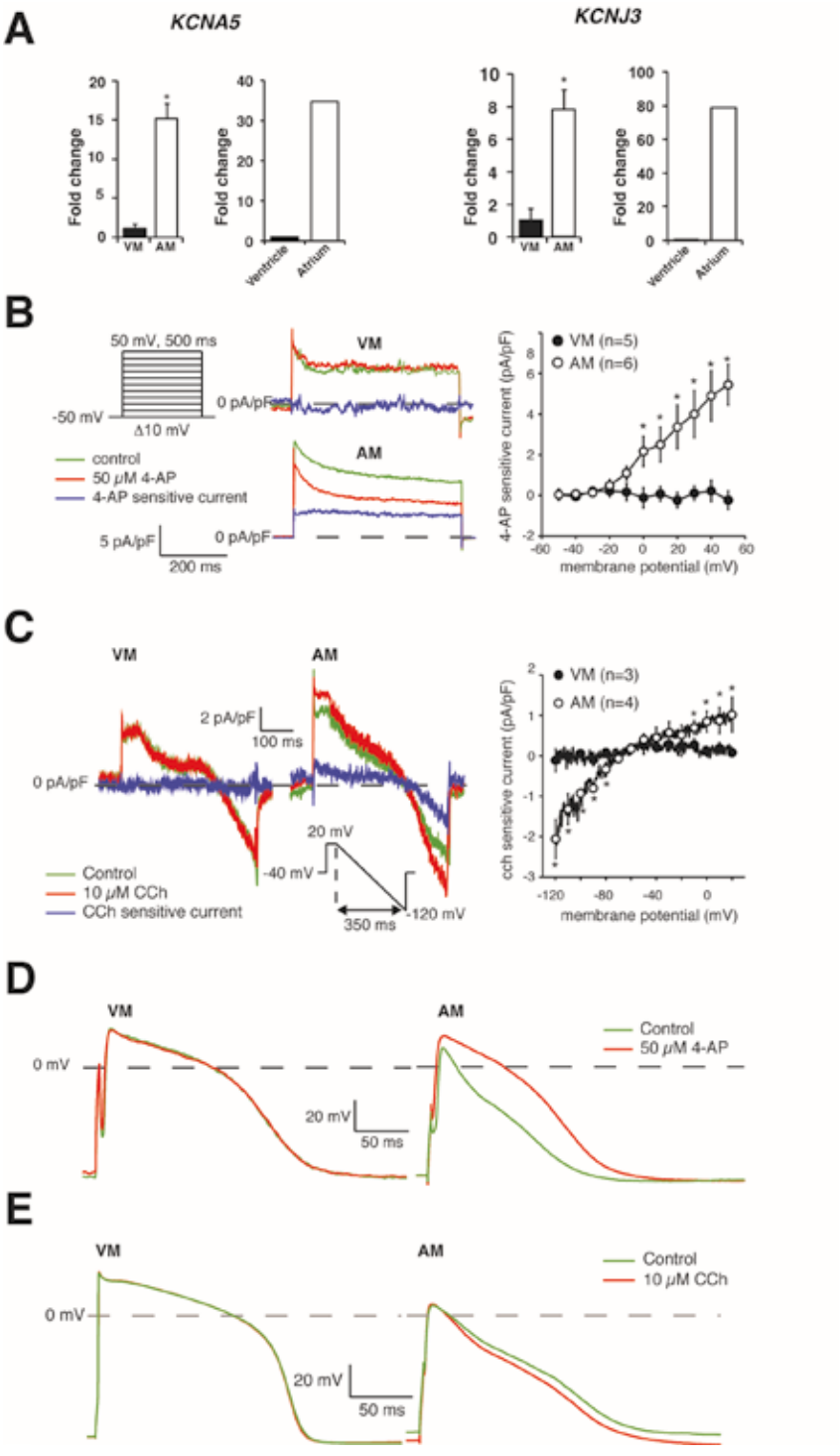
A
KCNA5
KCNJ3
Fold change
VM
AM
Ventricle
Atrium
B
50 mV, 500 ms
-50 mV
Δ10 mV
VM
AM
0 pA/pF
control
50 μM 4-AP
4-AP sensitive current
5 pA/pF
200 ms
VM (n=5)
AM (n=6)
4-AP sensitive current (pA/pF)
membrane potential (mV)
C
VM
AM
2 pA/pF
100 ms
0 pA/pF
20 mV
-40 mV
-120 mV
350 ms
Control
10 μM CCh
CCh sensitive current
VM (n=3)
AM (n=4)
cch sensitive current (pA/pF)
membrane potential (mV)
D
VM
AM
0 mV
20 mV
50 ms
Control
50 μM 4-AP
E
VM
AM
0 mV
20 mV
50 ms
Control
10 μM CCh

Figure 3.6: Characterization of I_{Kur} and $I_{K,ACh}$ in hESC-ventricular and hESC-atrial CMs. A) Expression of *KCNA5* (left) and *KCNJ3* (right) in GFP^+ pools of VM and AM CMs at day 31, as well as in ventricles and atria of human heart. *P<0.05 by unpaired t-test. B and C) Typical examples (left) and current-voltage relationships (right) of B) I_{Kur} and C) $I_{K,ACh}$ in VM and AM CMs. D-E) Representative APs of VM and AM at 1 Hz in response to D) I_{Kur} block by 4-AP and E) $I_{K,ACh}$ activation by CCh. AP parameters are shown in Expanded view table S5. CMs = cardiomyocytes; hESC-atrial (AM) and hESC-ventricular (VM) CMs; $I_{K,ACh}$ = acetylcholine-activated potassium current; I_{Kur} = potassium ultra-rapid delayed rectifier current. 4-AP = 4-aminopyridine; Carbachol = CCh. *P<0.05 by Two-Way Repeated Measures ANOVA followed by pairwise comparison using the Student-Newman-Keuls test for Fig. 3.6B and Mann-Whitney rank sum test for Fig. 3.6C.

Effects of vernakalant on APs of hESC-atrial and hESC-ventricular CMs

To validate hESC-atrial CMs as a preclinical model for screening the selectivity of ion channel blockers, we tested the effects of antiarrhythmic agent, Vernakalant (Wettwer et al., 2013). Intravenous form of this drug has recently been approved by the European Medicines Agency for cardioversion of recent-onset AF (Savelieva et al., 2014). In order to study the effects of this compound on the APs of hESC-atrial and hESC-ventricular CMs, 30 µmol/L of the compound (Wettwer et al., 2013) was administered whilst the cells were paced at various frequencies (1-4 Hz) and compared with pre-drug controls. Fig. 3.7A shows typical APs of hESC-atrial and hESC-ventricular CMs at 1 Hz in the absence and presence of vernakalant. In hESC-atrial CMs, at a frequency of 1 Hz, vernakalant significantly reduced dV/dt_{max} (Fig. 3.7A), increased APA_{max} (>2.5 mV) and APA_{plat} (>20%) resulting in prolongation of early as well as late repolarization (APD_{20}: >7.5 ms; APD_{50}: >15 ms and APD_{90}: >22 ms) in hESC-atrial CMs. These effects on APA_{plat} and dV/dt were also observed at higher stimulation frequencies (Figs. 3.7B and C). In hESC-ventricular CMs, vernakalant reduced dV/dt_{max} but without affecting other AP parameters at 1 Hz (Fig 3.7A; Expanded view table S6). Interestingly, vernakalant depressed dV/dt_{max} in a frequency-dependent manner in both hESC-atrial and hESC-ventricular CMs by a similar amount (Fig. 3.7C). The AP changes in response to vernakalant were nearly reversible upon washout. The effects of 30 µmol/L vernakalant on dV/dt_{max}, APA and APD_{20}

of hESC-atrial CMs were consistent with the results observed in human atrial trabeculae in sinus rhythm (SR) (Wettwer et al., 2013).

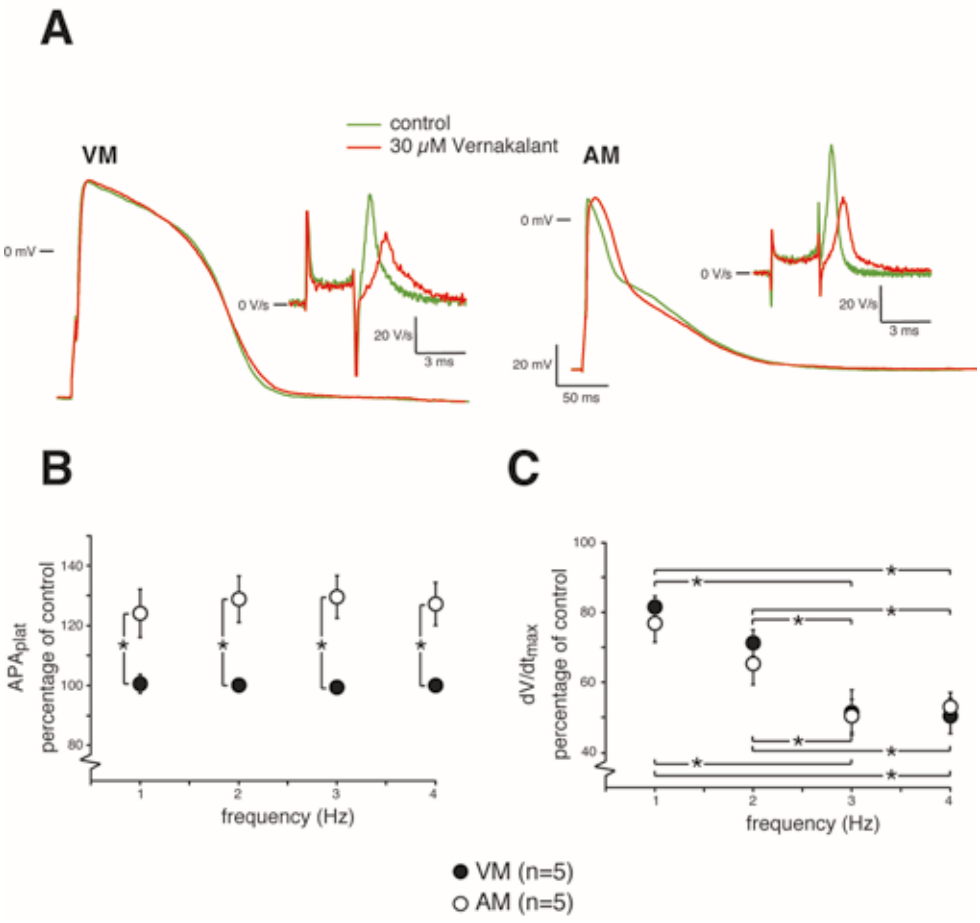

Figure 3.7: Effects of vernakalant on APs of hESC-ventricular and hESC-atrial CMs. A) Representative APs at 1 Hz of VM and AM CMs in response to vernakalant. Inset shows dV/dt_{max}. B) Average APA_{plat} and C) dV/dt_{max} in the absence and presence of vernakalant at 1-4 Hz. AP parameters are shown in Expanded view table S6. Abbreviations as in Figures 3.3 and 3.6. *P<0.05 by Mann-Whitney rank sum test for Fig. 7B; Two-Way Repeated Measures ANOVA followed by pairwise comparison using the Student-Newman-Keuls test for Fig. 3.7C.

Effects of XEN-D0101 on APs of hESC-atrial and hESC-ventricular CMs

Drugs developed to target $K_v1.5$ channels would ideally offer atrial selectivity and have no proarrhythmic effect, since IKur conducted by these channels is absent in the ventricles. To determine the response of hESC-atrial CMs to blockers that act on repolarizing potassium currents expressed preferentially in atrial CMs, we tested the effect of a selective $K_v1.5$ blocker, XEN-D0101 (Ford et al., 2013). Fig. 3.8A shows typical APs of hESC-atrial and hESC-ventricular CMs at 1 Hz in the absence and presence of 3 µmol/L XEN-D0101. Treatment with XEN-D0101 caused robust elevation of APA_{plat} (>26 mV) as well significant prolongation of APD_{20} (>30 ms), APD_{50} (>35 ms) and APD_{90} (>23 ms) in hESC-atrial cells but the compound did not significantly alter any AP parameter in hESC-ventricular CMs (Fig. 3.8A and Expanded view table S7). AP changes caused by XEN-D0101 were reversible upon washout. The effect of XEN-D0101 on APD_{20} and APD_{50} of hESC-atrial CMs is consistent with the effects observed in native human atrial trabeculae in SR (Ford et al., 2013). On the contrary, XEN-D0101 significantly altered APA (>10 mV) and dV/dt_{max} (>8 V/s) in hESC-atrial CMs compared with atrial trabeculae in SR. Intriguingly, XEN-D0101 prolonged APD_{90} in hESC-atrial CMs as well as in human atrial trabeculae (Ford et al., 2013) in AF while a reduction was observed in SR.

Effects of XEN-R0703 on APs of hESC-atrial and hESC-ventricular CMs

Enhanced parasympathetic tone and constitutive-activation of $I_{K,ACh}$ are believed to be contributing factors to both paroxysmal AF (clinically termed 'vagal AF') and chronic AF in man (Dobrev et al., 2005). Thus, antiarrhythmic drugs targeting the Kir3.1/3.4 channels are a promising therapeutic option for AF termination and the maintenance of SR. To determine the presence of $I_{K,ACh}$ in hESC-atrial and hESC-ventricular CMs, we tested XEN-R0703, a novel selective $I_{K,ACh}$ blocking antiarrhythmic drug. The ion channel pharmacology of XEN-R0703 was investigated in HEK293 cells or CHO cells expressing the channel of interest (Expanded view table S8; Fig. S7). XEN-R0703 potently inhibited recombinant Kir3.1/3.4 (IC_{50} =57 nM, nH = 0.52 ± 0.1) and had nominal effect on other cardiac channels displaying

100-fold selectivity over hERG (IC_{50} 5.6 µM, nH = 0.99 ±0.2) and >300-fold selectivity over $Na_v1.5$, $Ca_v1.2$ and Kir2.1 (IC_{50} >> 10 µM for each) (Fig. S7 and Expanded view table S8). The effect of XEN-R0703 on native human $I_{K,ACh}$ was investigated in HEK293 cells or CHO cells expressing the channel of interest (Expanded view table S8; Fig. S7). XEN-R0703 potently inhibited recombinant Kir3.1/3.4 (IC_{50} =57 nM, nH = 0.52 ± 0.1) and had nominal effect on other cardiac channels displaying 100-fold selectivity over hERG (IC_{50} 5.6 µM, nH = 0.99 ±0.2) and >300-fold selectivity over $Na_v1.5$, $Ca_v1.2$ and Kir2.1 (IC_{50} >> 10 µM for each) (Fig. S7 and Expanded view table S8). The effect of XEN-R0703 on native human $I_{K,ACh}$ was confirmed using primary human atrial CMs. 300 nM XEN-R0703 inhibited the CCh-activated native human $I_{K,ACh}$ by 81 ±10 % (Fig. S8).

To study the effect of 1 µmol/L XEN-R0703 on APs of hESC-atrial and hESC-ventricular CMs, $I_{K,ACh}$ current was first activated with 10 µmol/L CCh as shown in Fig. 3.6, followed by addition of XEN-R0703. Fig. 3.8B shows typical APs of hESC-atrial and hESC-ventricular CMs at 1 Hz in the absence and presence of XEN-R0703 as well as in the continuous presence of CCh. XEN-R0703 reversibly depolarized the RMP and restored the AP shortening caused by CCh in hESC-atrial CMs (Expanded view table S9). In contrast to hESC-atrial CMs, XEN-R0703 did not affect any AP parameter in hESC-ventricular CMs, consistent with the absence of $I_{K,ACh}$ in these cells. These results also demonstrate that XEN-R0703 does not affect other membrane currents present in hESC-ventricular CMs, consistent with the effects of the drug observed in HEK-293 cells expressing various ion channels (Expanded view table S8, Fig. S7). In order to confirm the selectivity of XEN-R0703 predicted by the effect on hESC-atrial CMs *in vitro,* the effect of XEN-R0703 was studied in an *in vivo* RAP dog model of persistent AF. XEN-R0703 increased right atrial effective refractory period (AERP) in dog by 10 %, 17 % and 28 % at 1, 3 and 10 mg/kg without affecting the Van de Water's QT_c-interval (Fig 3.8C). Furthermore, as depicted in Fig 3.8D, XEN-R0703 reduced AF inducibility from 76 % in vehicle to 43% and 11% following administration of 3 and 10 mg/kg.

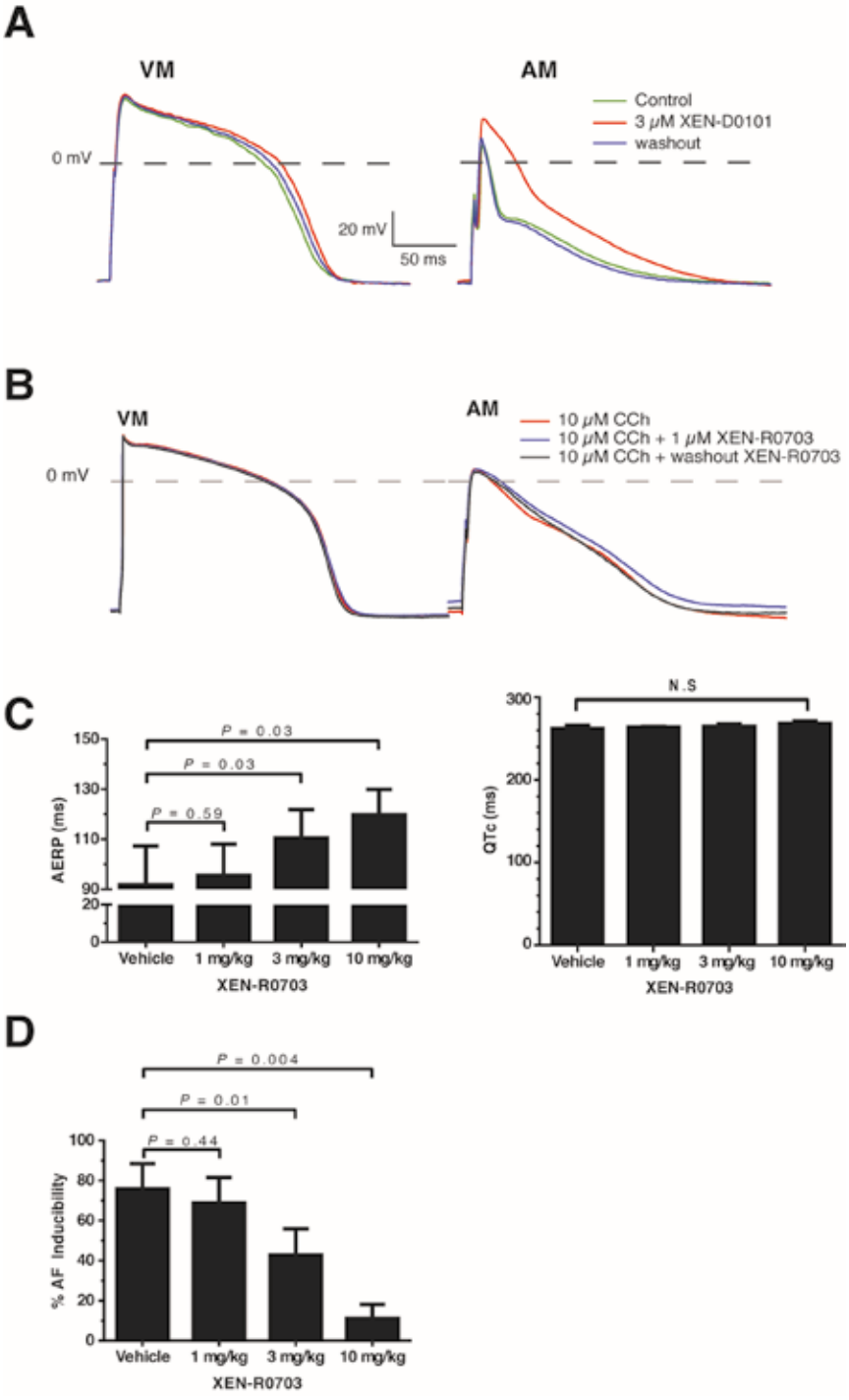
A
VM
AM
Control
3 μM XEN-D0101
washout
0 mV
20 mV
50 ms
B
VM
AM
10 μM CCh
10 μM CCh + 1 μM XEN-R0703
10 μM CCh + washout XEN-R0703
0 mV
C
P = 0.03
P = 0.03
P = 0.59
AERP (ms)
150
130
110
90
20
0
Vehicle
1 mg/kg
3 mg/kg
10 mg/kg
XEN-R0703
N.S
QTc (ms)
300
200
100
0
Vehicle
1 mg/kg
3 mg/kg
10 mg/kg
XEN-R0703
D
P = 0.004
P = 0.01
P = 0.44
% AF Inducibility
100
80
60
40
20
0
Vehicle
1 mg/kg
3 mg/kg
10 mg/kg
XEN-R0703

Figure 3.8: Effects of XEN-D0101 and XEN-R0703 on APs of hESC-ventricular and hESC-atrial CMs. A) Representative APs of VM and AM CMs in the absence, presence and following washout of 3 μmol/L XEN-D0101. AP parameters are shown in Expanded view table S7. B) Representative APs (1 Hz) of VM and AM in the CCh, to activate $I_{K,ACh}$ and subsequent addition of XEN-R0703. AP parameters are shown in Expanded view table S9. C and D) Experiments performed in RAP conscious dogs in the presence of vehicle or following 1, 3, 10 mg/kg XEN-R0703 show C) mean right AERP values (left), mean Van de Water's QT_c (right) and D) AF inducibility plotted as a function of dose; AERP = atrial effective refractory period; AF = atrial fibrillation; RAP = rapid atrial pacing; N.S = Not significant. Other abbreviations as in figures 3.3, 3.6 and 3.7. For RAP dog experiments, n=5; Statistical significance tested with paired t-test.

Discussion

Despite the remarkable improvement in efficiency and robustness of protocols for cardiac differentiation of hPSCs, the resulting CM population is usually a heterogeneous pool of atrial-, ventricular- and nodal-like cells (Mummery et al., 2012). Native atrial and ventricular CMs exhibit distinct molecular and functional profiles essential for their diverse physiological roles in the heart and hPSC-CM cultures enriched in these subtypes would have significant added value in drug response assays.

In the study described here, we directed hESCs towards atrial-like CMs by exogenous addition of RA during CM differentiation. RA signaling is crucial for atrial chamber development *in vivo* (Hochgreb et al., 2003; Niederreither et al., 2001) and its activation has previously been shown to steer differentiation of mouse and human ESCs towards atrial-like CMs (Gassanov et al., 2008; Zhang et al., 2011). However, little is known about the molecular mediators that govern ion channel repertoire of RA-driven atrial-like CMs and their suitability as a model system for preclinical drug screenings. Gene expression profiling of the resulting CMs, exposed to RA during differentiation, indicated an upregulation of atrial transcripts such as *COUP-TFII, SLN, NPPA* and *PITX2* along with a downregulation of ventricular transcripts such as *HAND1, HEY2, IRX4* and *MYL2*. COUP-TFII is expressed in atrial chambers of the heart and has been reported to determine atrial identity in mice (Wu et al., 2013). SLN is also atrial-specific and is an integral part of the sarcoplasmic reticulum calcium complex (Minamisawa et al., 2003). NPPA is expressed in both atrial and ventricular chambers during development and becomes progressively restricted to the atria shortly after birth (De Sousa Lopes et al., 2006). Cardiac left-right determinant PITX2 is expressed in the left atrium and its insufficiency has been linked to atrial arrhythmogenesis (Kirchhof et al., 2011). Myosin light chain gene, MYL2 iroquois homeobox transcription factor, IRX4, basic helix-loop-helix transcription factors, HAND1 and HEY2 are expressed in the developing ventricles of the heart and have critical roles in ventricular chamber development and function (Moorman et al., 2003). Moreover, the global gene profile of hESC-atrial CMs showed a higher overlap with that of human fetal atria and hESC-ventricular CMs showed an increased overlap with that of human fetal ventricles. About 30% of the genes in GFP^+ cells of hESC-atrial or hESC-ventricular CMs overlapped with that of chamber-specific genes in the fetal heart. Taking into account that we used atria and

ventricles from a 15-week old human heart, consisting of cardiomyocytes, endothelial cells, smooth muscle cells, fibroblasts and other cardiac cells, a 30% overlap can be considered as a strong correlation. An additional limiting factor is the stage of heart used for microarray analysis. We used a second trimester human fetal heart for comparison to hESC-derived CMs while a previous study has noted that ESC-derived CMs resemble that of embryonic heart tube (Fijnvandraat et al., 2003). Multiple mechanisms such as transcriptional regulation or programmed cell death leading to selective survival, might contribute to subtype specification of atrial or ventricular CMs. Earlier studies in amniotes had suggested a possibility that RA is required for the formation of atrial cardiomyocytes and that in its absence, cardiac precursors differentiate to ventricular cells (Hochgreb et al., 2003; Simões-Costa et al., 2005). However, a recent study in zebrafish has shown that RA signaling acts via different mechanisms to limit both atrial and ventricular cell numbers but not at the expense of each other (Waxman et al., 2008). In the current study, we did not observe any unusual apoptosis in RA-treated EBs compared to controls during hPSC differentiation. Moreover, we observed rapid and robust induction of COUP-TFs in response to RA and thus proposed a central role for these transcription factors in RA-driven atrial differentiation. COUP-TFI and COUP-TFII belong to the steroid receptor super family of genes and display overlapping yet distinct patterns of expression in all the three germ layers in mouse (Pereira et al., 2000). Both these COUP-TF genes are induced by retinoids *in vivo* in zebrafish brain (Jonk et al., 1994). In addition, determination of the crystal structure of COUP-TFII led to its identification as a RA activated receptor (Kruse et al., 2008). Interestingly, deletion of either RALDH2 or COUP-TFII in the mouse results in severe abnormalities of the atria and sinus venosus, implicating COUP-TFII as a possible downstream effector of RA-driven posterior chamber specification. While a role for COUP-TFII in the heart and vasculature has been identified, little is known about the function of COUP-TFI in the heart. COUP-TFI was found to be expressed in whole heart protein lysates obtained from embryonic and neonatal mouse hearts and has been proposed to antagonize the activation of Calreticulin promoter by NKX2.5 (Guo et al., 2001). The localization of COUP-TFI in the human heart and its role in cardiac lineage specification has been unknown to date. We showed here that COUP-TFI is induced by RA along with COUP-TFII during atrial differentiation *in vitro* and was also expressed specifically in the atrial chambers of the human heart. It is worth mentioning that COUP-TFI was observed only in the atria of the human fetal heart while expression

of COUP-TFII spanned a broader region (endothelium, smooth muscle cells-data not shown) than just the atria suggesting non-redundant functions of these genes in the human heart.

Based on our results as well as evidence from previous studies pointing to an integral role for COUP-TFs in the retinoid network and cell-fate determination, we investigated the functional significance of robust expression of these genes in hESC-atrial CMs. shRNA-mediated knockdown as well as ChIP experiments demonstrated that COUP-TFs regulate the atrial-selective ion channel gene, *KCNA5*. These experiments also established that *KCNJ3* and *KCNJ5* are regulated by COUP-TFII. Interestingly, although COUP-TFI showed strong interaction with the *KCNJ3* promoter, knockdown of COUP-TFI itself did not result in a decrease in the expression of *KCNJ3*. This suggests that COUP-TFI might be dispensable for the expression of *KCNJ3* and *KCNJ5* in atrial CMs. Future studies aimed at dissecting the roles of COUP-TFI and COUP-TFII during atrial differentiation are required to understand whether these genes act in synergy or possess functions independent and specific to one another. It also remains to be tested if loss of COUP-TFI can be rescued by COUP-TFII and vice versa. However, since myocardial ablation of COUP-TFII in the mouse results in a severe phenotype (Wu et al., 2013), it seems unlikely that COUP-TFI can account for loss of COUP-TFII. Nonetheless, it is likely that deletion of both COUP-TFI and COUP-TFII might result in a more severe phenotype. Ion channels $K_v1.5$, Kir3.1 and Kir3.4 encoded by *KCNA5, KCNJ3* and *KCNJ5* respectively, conduct the potassium currents I_{Kur} and $I_{K,ACh}$ which are major determinants of electrophysiological differences between atrial and ventricular CMs in humans (Ravens et al., 2013; Schram et al., 2002). Although mechanisms controlling ion channel expression are far more complex than transcriptional regulation alone, these findings identify a potential regulatory mechanism of *KCNA5* and *KCNJ3* in human atrial myocytes. Previous work by others has shown that COUP-TFs regulate the expression of Na^+/H^+exchanger (NHE) in differentiating P19 cells (Fernandez-Rachubinski and Fliegel, 2001). The ability of these transcription factors to regulate ion channels in diseased and non-diseased human heart warrants further investigation to better understand their role in pathophysiological states. In addition to identifying a central role for COUP-TFs in the transcriptional regulation of *KCNA5* and *KCNJ3*, we also reported the functional presence of potassium currents encoded by these atrial-specific ion channel genes, in hESC-atrial but not hESC-ventricular CMs. These findings prompted us to investigate whether hESC-atrial

CMs would be a suitable model for preclinical testing of pharmacological compounds currently being developed for AF. Drug responses of hESC-atrial CMs following treatment with multiple ion channel blocker, vernakalant and selective $K_v1.5$ blocker, XEN-D0101 recapitulated the effects observed on early repolarization in human right atrial trabeculae in SR (Ford et al., 2013; Wettwer et al., 2013). Furthermore, we observed effects of these compounds on other AP parameters such as APD_{90} in hESC-atrial CMs that differ from those previously reported in human atrial trabeculae in SR. This may be due to the use of dialysed (whole-cell patch-clamp) single cells in this study, whereas previous studies used multicellular preparations, in which cells were non-dialysed (sharp microelectode) and electrically coupled. Additionally, we tested a novel Kir3.1/3.4 blocker, XEN-R0703 in an *in vivo* RAP dog model. Dog is regarded as the one of the most predictive animal species of human cardiovascular toxicity and is routinely used in the pharmaceutical industry to assess cardiac safety and the risk of drug-induced ventricular arrhythmias (Olson et al., 2000). In the dog, XEN-R0703 resulted in a dose-dependent increase of AERP without affecting the QT_c interval. These results suggest lack of effect of XEN-R0703 on the ventricles and confirm its atrial selectivity as predicted in hESC-atrial CMs. hPSC-derived CMs are spontaneously active and exhibit depolarized RMP. Evidence suggests that they are developmentally immature, resembling human fetal CMs rather than their adult counterparts (Beqqali et al., 2006). In our study, RMP did not differ between hESC-atrial CMs and hESC-ventricular CMs indicating similar level of maturity in both the groups. Nonetheless, hESC-atrial CMs respond to atrial-selective ion channel blockers demonstrating that an immature electrical phenotype does not preclude their use in preclinical drug screening and pharmacology. Our findings have important implications for integrating hPSC-derived atrial CMs into high-throughput screenings for selection and validation of lead compounds during early stages of drug discovery.

In conclusion, we addressed the void for a humanized preclinical screening platform in the pharmaceutical industry for evaluating selectivity of novel ion channel blockers for AF. We showed that hESC-atrial CMs respond to atrial-selective compounds in a manner similar to isolated human atrial CMs thus demonstrating the potential of this tool as a robust model for preclinical atrial-selective pharmacology.

Materials and Methods

HESC culture and differentiation to CMs

A transgenic NKX2.5$^{eGFP/+}$ hESC line that faithfully reports endogenous NKX2.5 expression by GFP was described previously (Elliott et al., 2011). Undifferentiated hESCs were maintained on irradiated mouse embryonic fibroblasts and cardiac differentiation was induced using a spin EB protocol. Briefly, hESCs were harvested and resuspended on day-0 in BPEL medium (Ng ES, Davis R, Stanley EG, 2008) containing 20-30 ng/ml hActivin-A (R&D systems), 20-30 ng/ml bone morphogenetic protein 4 (R&D systems), 40 ng/ml stem cell factor (Stem cell technologies), 30 ng/ml vascular endothelial growth factor (R&D systems) and 1.5 µmol/L CHIR 99021 (Axon Medchem). EBs were refreshed on day 3 with BPEL and then transferred to gelatin-coated dishes on day 7. To induce atrial specification in hESCs, cardiac differentiation was initiated as described above and 1 µmol/L all-trans retinoic acid (RA) (Sigma) was added on day 4 of differentiation. Cells were refreshed with BPEL on day 7 of differentiation.

Cellular Electrophysiology

Cell preparation, data acquisition and analysis: Spin EBs resulting from control and RA-treated differentiations were dissociated at day 17 to single cells using TrypLE™ Select (Life technologies) and plated on gelatin-coated coverslips. Electrophysiological measurements were performed 10-14 days after dissociation from intrinsically quiescent single GFP$^+$ CMs that were able to contract upon field stimulation.

APs and membrane currents from hESC-CMs were recorded with the amphotericin-B-perforated patch-clamp technique at 36 ±0.2°C using an Axopatch 200B amplifier (Molecular Devices, Sunnyvale, CA, USA). Cells were superfused with Tyrode's solution containing (in mmol/L): NaCl 140, KCl 5.4, $CaCl_2$ 1.8, $MgCl_2$ 1.0, glucose 5.5, and HEPES 5.0; pH was adjusted to 7.4 with NaOH. Pipettes (borosilicate glass; resistance 2–3 MW) were heat polished and filled with solution containing (in mmol/L): K-gluconate 125, KCl 20, NaCl 5, amphotericin-B 0.22, and HEPES 10; pH was adjusted to 7.2 with KOH. AP measurements were low-pass filtered (cut-off frequency 10

kHz) and digitized at 40 kHz; membrane currents were measured at 1 kHz and 4 kHz, respectively. Capacitance and series resistance was compensated by ≥80%, and APs were corrected for the calculated liquid junction potential (Barry and Lynch, 1991). Voltage control, data acquisition, and analysis were accomplished using custom software. Cell membrane capacitance (Cm) was estimated by dividing the time constant of the decay of the capacitive transient in response to 5 mV hyperpolarizing voltage clamp steps from –40 mV by the series resistance.

Current clamp experiments: APs were elicited at 0.5 to 4 Hz by 3 ms, ~1.2´ threshold current pulses through the patch pipette. APs were characterized, as depicted in Fig. 2A, by resting membrane potential (RMP), maximum upstroke velocity (dV/dt_{max}), maximum AP amplitude (APA_{max}), AP plateau amplitude (APA_{plat}, defined as the potential difference between RMP and potential at 20 ms after the upstroke), and the duration at 20, 50, and 90% repolarization (APD_{20}, APD_{50}, and APD_{90} respectively). Parameter values obtained from 10 consecutive APs were averaged.

Voltage clamp experiments: The ultrarapid delayed rectifier K^+ current (I_{Kur}) and the acetylcholine-activated K^+ current ($I_{K,ACh}$) were measured as the current sensitive to 50 μM 4-aminopyridine (4-AP) or 10 μM carbachol (CCh), respectively, in the presence of 10 μM nifedipine to block the L-type Ca^{2+} current. Voltage-clamp protocols are shown in the corresponding figures and have been described previously (Barry and Lynch, 1991). Current density was calculated by dividing current amplitude by Cm.

Statistics

qPCR, electrophysiology, pharmacology, ChIP and knockdown experiments were performed on cardiomyocytes resulting from three independent control and RA-treated differentiations. Statistical analysis was carried out with SigmaStat 3.5 software. Normality and equal variance assumptions were tested with the Kolmogorov-Smirnov and the Levene median test, respectively. Groups were compared with unpaired t-test or with Mann-Whitney Rank Sum Test (in case of a failed normality and/or equal variance test). Two-Way Repeated Measures (RM) ANOVA followed by the Student-Newman-Keuls post hoc test was used by comparing groups in the frequency and I-V

relationships. In case of a failed normality and/or equal variance test, data were tested with the Mann-Whitney Rank Sum Test per frequency or voltage. Paired t-tests, was used to compare drug effects within a group of cells. Data obtained at a series of frequencies within a group were compared with one-way RM ANOVA. Groups were compared using paired/unpaired t-test or Two-Way Repeated Measures ANOVA followed by pairwise comparison using the Student-Newman-Keuls test. $P<0.05$ defines statistical significance. Data are presented as means ± SEM.

Ethics statement

Studies on hESCs were performed in the Netherlands and their use was approved by the medical ethical committee of Leiden University Medical Center (LUMC). Collection and use of human fetal material for research was also approved by the medical ethical committee of LUMC (protocol 08.087). Specimens of human atrial appendage were obtained from patients undergoing a range of cardiac surgical procedures with written informed consent and conformed to the principles outlined in the Declaration of Helsinki. Tissue was obtained from consenting patients (from Papworth Hospital NHS Trust, Cambridge, UK) following approval from the Local Research Ethical Approval Committee (H03/035). Animal experiments were carried out by CorDynamics, IL, USA, in compliance with the Guide for the Care and Use of Laboratory Animals (U.S.A.NIH publication No 85-23, revised 1985).

Acknowledgements

Funding for this study from the following sources is gratefully acknowledged: Netherlands Organization for health research and development (ZonMw-TOP 40-00812-98-12086) to H.D.D. and (ZonMw-MKMD-40-42600-98-036) to R.P; Leiden University Medical Center (BW-plus) doctoral grant to V.R.; European Union (FP7-Health T2-2010-261057 "EUTRAF") to Xention Ltd. (J.W.F., J.T.M., C.J., S.E-H); Netherlands Heart Foundation (NHS 2008B106) to K.G.; Netherlands Organization for Scientific Research-(NWO-ASPASIA 016.121.365) and Interuniversity Attraction Poles Program (IUAP-07/07) to S.M.C.d.S.L.; European Research Council advanced grant (STEMCARDIOVASC-323182) to C.L.M.

The authors thank Dr Milena Bellin for critical reading of the manuscript and CASA (Leiden and Den Haag) for the collection of human fetal material.

Conflict of interest

Authors H.D.D., V.S., K.G., D.A.E., S.M.C.d.S.L and A.O.V. have nothing to disclose. C.L.M. and R.P. are co-founders and advisors of Pluriomics. J.W.F., J.T.M., S.E.H. and C.J. are employees of Xention Ltd and hold stock/stock-options in Xention Ltd.

References

Barry PH, Lynch JW. Liquid junction potentials and small cell effects in patch-clamp analysis. J Membr Biol 1991; 121:101–117.

Beqqali A, Kloots J, Ward-van Oostwaard D, Mummery C, Passier R. Genome-Wide Transcriptional Profiling of Human Embryonic Stem Cells Differentiating to Cardiomyocytes. Stem Cells 2006; 24:1956–1967.

Blazeski A, Zhu R, Hunter DW, Weinberg SH, Boheler KR, Zambidis ET, Tung L. et al., Electrophysiological and contractile function of cardiomyocytes derived from human embryonic stem cells. Prog Biophys Mol Biol 2012; 110:178–195.

Braam SR, Tertoolen L, van de Stolpe A, Meyer T, Passier R, Mummery CL. Prediction of drug-induced cardiotoxicity using human embryonic stem cell-derived cardiomyocytes. Stem Cell Res 2010; 4:107–116.

Choisy SPCM, James AF, Hancox JC. Acute desensitization of acetylcholine and endothelin-1 activated inward rectifier K+ current in myocytes from the cardiac atrioventricular node. Biochem Biophys Res Commun 2012; 423:496–502.

Chugh SS, Havmoeller R, Narayanan K, Singh D, Rienstra M, Benjamin EJ, Gillum RF, Kim YH, McAnulty JH Jr, Zheng ZJ. et al., Worldwide Epidemiology of Atrial Fibrillation: A Global Burden of Disease 2010 Study. Circulation 2014; 129:837–847.

Chuva de Sousa Lopes SM, Hassink RJ, Feijen A, van Rooijen MA, Doevendans PA, Tertoolen L, Brutel de la Rivière A, Mummery CL. et al., Patterning the heart, a template for human cardiomyocyte development. Dev Dynam 2006; 235:1994–2002.

Dobrev D, Friedrich A, Voigt N, Jost N, Wettwer E, Christ T, Knaut M, Ravens U. et al., The G Protein-Gated Potassium Current IK,ACh Is Constitutively Active in Patients With Chronic Atrial Fibrillation. Circulation 2005; 112:3697–3706.

Dobrev D, Nattel S. New antiarrhythmic drugs for treatment of atrial fibrillation. The Lancet 2010; 375:1212–1223.

Elliott DA, Braam SR, Koutsis K, Ng ES, Jenny R, Lagerqvist EL, Biben C, Hatzistavrou T, Hirst CE, Yu QC. et al., NKX2-5(eGFP/w) hESCs for isolation of human cardiac progenitors and cardiomyocytes. Nat Methods 2011; 8:1037–1040.

Fernandez-Rachubinski F, Fliegel L. COUP-TFI and COUP-TFII regulate expression of the NHE through a nuclear hormone responsive element with enhancer activity. Eur J Biochem. 2001; 268:620–634.

Fijnvandraat AC, van Ginneken AC, de Boer PA, Ruijter JM, Christoffels VM, Moorman AF, Lekanne Deprez RH. et al., Cardiomyocytes derived from embryonic stem cells resemble cardiomyocytes of the embryonic heart tube. Cardiovasc. Res 2003; 58(2):399-409.

Ford J, Milnes J, Wettwer E, Christ T, Rogers M, Sutton K, Madge D, Virag L, Jost N, Horvath Z. et al., Human electrophysiological and pharmacological properties of XEN-D0101: A novel atrial selective Kv1. 5/I Kur inhibitor. J Cardiovasc Pharm 2013; 61(5):408-15.

Gassanov N, Er F, Zagidullin N, Jankowski M, Gutkowska J, Hoppe UC. Retinoid acid induced effects on atrial and pacemaker cell differentiation and expression of cardiac ion channels. Differentiation 2008; 76:971–980.

Guo L, Lynch J, Nakamura K. et al, Fliegel L, Kasahara H, Izumo S, Komuro I, Agellon LB, Michalak M. et al., COUP-TF1 antagonizes Nkx2.5-mediated activation of the calreticulin gene during cardiac development. J Biol Chem 2001; 276:2797–2801.

Hochgreb T, Linhares VL, Menezes DC, Sampaio AC, Yan CY, Cardoso WV, Rosenthal N, Xavier-Neto J. et al., A caudorostral wave of RALDH2 conveys anteroposterior information to the cardiac field. Development 2003; 130:5363–5374.

Jonk LJC, de Jonge MEJ, Vervaart JMA, Wissink S, Kruijer W. Isolation and developmental expression of retinoic-acid-induced genes. Devl Biol 1994;

Keegan BR, Feldman JL, Begemann G, Ingham PW, Yelon D. Retinoic acid signaling restricts the cardiac progenitor pool. Science 2005; 307:247–249.

Kirchhof P, Kahr PC, Kaese S, Piccini I, Vokshi I, Scheld HH, Rotering H, Fortmueller L, Laakmann S, Verheule S. et al.,

PITX2c is expressed in the adult left atrium, and reducing Pitx2c expression promotes atrial fibrillation inducibility and complex changes in gene expression. Circ Cardiovasc Genet 2011; 4:123–133.

Koumi S, Arentzen CE, Backer CL, Wasserstrom JA. Alterations in muscarinic K+ channel response to acetylcholine and to G protein-mediated activation in atrial myocytes isolated from failing human hearts. Circulation 1994; 90:2213–2224.

Krapivinsky G, Gordon EA, Wickman K, Velimirovic B, Krapivinsky L, Clapham DE. The G-protein-gated atrial K+ channel IKACh is a heteromultimer of two inwardly rectifying K(+)-channel proteins. Nature 1995; 374:135–141.

Kruse SW, Suino-Powell K, Zhou XE, Kretschman JE, Reynolds R, Vonrhein C, Xu Y, Wang L, Tsai SY, Tsai MJ. et al., Identification of COUP-TFII orphan nuclear receptor as a retinoic acid-activated receptor. PLoS Biol 2008; 6(9):e227.

Li D, Sun H, Levesque P. Antiarrhythmic drug therapy for atrial fibrillation: focus on atrial selectivity and safety. Cardiovasc Hematol Agents Med Chem 2009; 7:64–75.

Marini C, De Santis F, Sacco S, Russo T, Olivieri L, Totaro R, Carolei A. et al., Contribution of Atrial Fibrillation to Incidence and Outcome of Ischemic Stroke: Results From a Population-Based Study. Stroke 2005; 36:1115–1119.

Milnes JT, Madge DJ, Ford JW. New pharmacological approaches to atrial fibrillation. Drug Discov Today 2012; 17:654–659.

Minamisawa S, Wang Y, Chen J, Ishikawa Y, Chien KR, Matsuoka R. Atrial chamber-specific expression of sarcolipin is regulated during development and hypertrophic remodeling. J Biol Chem 2003; 278(11):9570-5.

Moorman AFM, Christoffels VM. Cardiac chamber formation: development, genes, and evolution. Physiol Rev 2003; 83:1223–1267.

Mummery CL, Zhang J, Ng ES, Elliott DA, Elefanty AG, Kamp TJ. Differentiation of Human Embryonic Stem Cells and Induced Pluripotent Stem Cells to Cardiomyocytes: A Methods Overview. Circ Res 2012; 111:344–358.

Navarrete EG, Liang P, Lan F, Sanchez-Freire V, Simmons C, Gong T, Sharma A, Burridge PW, Patlolla B, Lee AS. et al., Screening Drug-Induced Arrhythmia Events Using Human Induced Pluripotent Stem Cell–Derived Cardiomyocytes and Low-Impedance Microelectrode Arrays. Circulation 2013; 128:S3-S13

Nerbonne JM, Kass RS. Molecular physiology of cardiac repolarization. Physiol Rev 2005; 85:1205–1253.

Ng ES, Davis R, Stanley EG, Elefanty AG. A protocol describing the use of a recombinant protein-based, animal product-free medium (APEL) for human embryonic stem cell differentiation as spin embryoid bodies. Nat Protoc 2008; 3:768–776.

Niederreither K, Vermot J, Messaddeq N, Schuhbaur B, Chambon P, Dollé P. Embryonic retinoic acid synthesis is essential for heart morphogenesis in the mouse. Development 2001; 128:1019–1031

Olson H, Betton G, Robinson D, Thomas K, Monro A, Kolaja G, Lilly P, Sanders J, Sipes G, Bracken W. et al., Concordance of the toxicity of pharmaceuticals in humans and in animals. Regul Toxicol Pharmacol. 2000; 32: 56–67

Pereira FA, Qiu Y, Zhou G, Tsai MJ, Tsai SY. The orphan nuclear receptor COUP-TFII is required for angiogenesis and heart development. Genes Dev 1999; 13:1037–1049.

Pereira FA, Tsai MJ, Tsai SY. COUP-TF orphan nuclear receptors in development and differentiation. Cell Mol Life Sci 2000; 57:1388–1398.

Ravens U, Poulet C, Wettwer E, Knaut M. Atrial selectivity of antiarrhythmic drugs. J Physiol 2013; 591: 4087-4097.

Savelieva I, Graydon R, Camm AJ. Pharmacological cardioversion of atrial fibrillation with vernakalant: evidence in support of the ESC Guidelines. Europace 2014; 16:162–173.

Schram G, Pourrier M, Melnyk P, Nattel S. Differential distribution of cardiac ion channel expression as a basis for regional specialization in electrical function. Circ Res 2002; 90:939–950.

Simoes-Costa MS, Vasconcelos M, Sampaio AC, Cravo RM, Linhares VL, Hochgreb T, Yan CY, Davidson B, Xavier-Neto J. et al., The evolutionary origins of cardiac chambers. Devl Biol 2005; 277:1-15.

van der Wees J, Matharu PJ, de Roos K, Destrée OH, Godsave SF, Durston AJ, Sweeney GE. et al., Developmental expression and differential regulation by retinoic acid of Xenopus COUP-TF-A and COUP-TF-B. Mech Dev 1996; 54:173–184.

Wang TJ, Larson MG, Levy G, Vasan RS, Leip EP, Wolf PA, D'Agostino RB, Murabito JM, Kannel WB, Bemjamin EJ. Temporal Relations of Atrial Fibrillation and Congestive Heart Failure and Their Joint Influence on Mortality: The Framingham Heart Study. Circulation 2003; 107:2920–2925.

Wang Z, Fermini B, Nattel S. Sustained depolarization-induced outward current in human atrial myocytes. Evidence for a novel delayed rectifier K+ current similar to Kv1.5 cloned channel currents. Circ Res 1993; 73:1061–1076.

Wann LS, Curtis AB, January CT, Ellenbogen KA, Lowe JE, Estes NA 3rd, Page RL, Ezekowitz

MD, Slotwiner DJ, Jackman WM. et al., 2011 ACCF/AHA/HRS Focused Update on the Management of Patients With Atrial Fibrillation(Updating the 2006 Guideline). J Am Coll Cardiol 2011; 57:223–242.

Waxman JS, Keegan BR, Roberts RW, Poss KD, Yelon D. Hox5b acts downstream of retinoic acid signaling in the forelimb field to restrict heart field potential in zebrafish. Dev. Cell 2008; 15(6):923-34.

Wettwer E, Christ T, Endig S, Rozmaritsa N, Matschke K, Lynch JJ, Pourrier M, Gibson JK, Fedida D, Knaut M. et al., The new antiarrhythmic drug vernakalant: ex vivo study of human atrial tissue from sinus rhythm and chronic atrial fibrillation. Cardiovascular Research 2013; 98:145–154.

Wu S-P, Cheng C-M, Lanz RB, Wang T, Respress JL, Ather S, Chen W, Tsai SJ, Wehrens XH, Tsai MJ. et al., Atrial identity is determined by a COUP-TFII regulatory network. Dev Cell 2013; 25:417–426.

Zhang Q, Jiang J, Han P, Yuan Q, Zhang J, Zhang X, Xu Y, Cao H, Meng Q, Chen L. et al., Direct differentiation of atrial and ventricular myocytes from human embryonic stem cells by alternating retinoid signals. Cell Res 2011; 21:579–587.